RESEARCH MEMORANDUM

INVESTIGATION OF TWO-STAGE AIR-COOLED TURBINE SUITABLE FOR FLIGHT AT MACH NUMBER OF 2.5

II - BLADE DESIGN

By James W. Miser and Warner L. Stewart

Lewis Flight Propulsion Laboratory
Cleveland, Ohio

NATIONAL ADVISORY COMMITTEE
FOR AERONAUTICS

WASHINGTON

January 22, 1957

NATIONAL ADVISORY COMMITTEE FOR AERONAUTICS

RESEARCH MEMORANDUM

INVESTIGATION OF TWO-STAGE AIR-COOLED TURBINE SUITABLE FOR FLIGHT AT MACH NUMBER OF 2.5

II - BLADE DESIGN

By James W. Miser and Warner L. Stewart

SUMMARY

A blade design study is presented for a two-stage air-cooled turbine suitable for flight at a Mach number of 2.5 for which velocity diagrams have been previously obtained. The detailed procedure used in the design of the blades is given. In addition, the design blade shapes, surface velocity distributions, inner and outer wall contours, and other design data are presented.

Of all the blade rows, the first-stage rotor has the highest solidity, with a value of 2.289 at the mean section. The second-stage stator also had a high mean-section solidity of 1.927, mainly because of its high inlet whirl. The second-stage rotor has the highest value of the suction-surface diffusion parameter, with a value of 0.151. All other blade rows have values for this parameter under 0.100.

INTRODUCTION

The problems that arise in engines suitable for high flight speeds are being investigated at the NACA Lewis laboratory. As part of this program, a velocity-diagram study has been made of the turbine component of an axial-flow turbojet engine suitable for flight at a Mach number of 2.5 (ref. 1). On the basis of this study the free-stream velocity diagrams at the hub, mean, and tip and the inner and outer wall contours were obtained for a two-stage turbine that would satisfy the requirements of reference 1. These velocity diagrams are used to determine the velocity diagrams at the blade design section radii specified in the design procedure presented herein.

The purpose of the subject report is to present the results of a blade design study made for a turbine that would satisfy the requirements of reference 1. Included in this report are an outline of the blade design procedure, the final blade shapes and their coordinates, the blade

surface velocity distributions, and a discussion of some of the aerodynamic characteristics of the final blade shapes. Also discussed are the requirements imposed on the external blade shape by the amount of cooling air and by the type of cooling passages that might be employed to distribute the air and act as heat-transfer surfaces inside the blade. Since there may be changes in the internal blade cooling configuration in future experimental investigations, the effects of the cooling air on the mainstream flow are treated rather generally, and certain assumptions are made which allow for the increased mass flow but do not consider the many ways in which the cooling air could affect the flow inside and downstream of the blade channel.

SYMBOLS

b blade height, ft

C curvature, ft^{-1}

c blade chord length, ft

D_p pressure-surface diffusion parameter, defined as

$$\frac{\text{Blade inlet relative velocity - Minimum blade surface relative velocity}}{\text{Blade inlet relative velocity}}$$

D_s suction-surface diffusion parameter, defined as

$$\frac{\text{Maximum blade surface relative velocity - Blade-outlet relative velocity}}{\text{Maximum blade surface relative velocity}}$$

d approximate axial distance from trailing edge to center of channel exit, ft

l length (specified by subscript), ft

m slope of inner and outer walls

N number of blades

r radius, ft

r_C average radius of curvature of suction surface downstream of channel exit, ft

s blade spacing or pitch, ft

t trailing-edge thickness, ft

U blade velocity, ft/sec

V	absolute gas velocity, ft/sec
W	relative gas velocity, ft/sec
w	mass flow, lb/sec
α_s	blade stagger angle measured from axial direction, deg
β	relative gas-flow angle, deg
δ_{te}	trailing-edge-thickness parameter, t/(s cos β)
ρ	gas density, lb/cu ft
σ	blade solidity, c/s
ψ	angle equal to half the wedge angle at the blade trailing edge, deg
ω	rotative speed, radians/sec

Subscripts:

a	refers to axial station just inside trailing edge
av	average of suction- and pressure-surface quantities
c	center of channel exit
ce	channel exit
cr	conditions at Mach number of 1.0
h	hub
m	mean
mid	midchannel
o	orthogonal
p	pressure surface
s	suction surface
t	tip
x	axial

0 station at turbine entrance

1 station at outlet of first-stage stator

2 station at outlet of first-stage rotor

3 station at outlet of second-stage stator

4 station at outlet of second-stage rotor

Superscripts:

" relative total state

BLADE DESIGN CONSIDERATIONS

Turbine-Design Requirements

The design requirements of the subject turbine were determined in reference 1. The turbine velocity diagrams and the inner and outer wall contours which satisfy these requirements are reprinted in this report as figures 1 and 2(a), respectively.

Cooling-Air Requirements

The cooling-air requirements for each blade row are discussed in reference 1, where the cooling air required per blade row is given in terms of the ratio φ of turbine cooling-air to compressor inlet weight flow as follows:

First-stage stator, φ_1	0.025 (exhausted overboard)
First-stage rotor, φ_2	0.020
Second-stage stator, φ_3	0.025
Second-stage rotor, φ_4	0.020

Many ways of exhausting the turbine cooling air from the blades have been considered. Of these ways, the arrangement that seems most suitable for the proposed flight application is one in which the turbine cooling air from the first-stage stator is exhausted overboard and the cooling air of the other three blade rows is exhausted into the turbine mainstream flow. This arrangement seems to be feasible when the cooling air for the first- and second-stage rotors is exhausted from the tip end and the cooling air from the second-stage stator is exhausted from the hub end.

Effect of Internal Cooling-Passage Requirements on Design of External Blade Shapes

In designing an internally cooled blade, adequate provisions for the internal blade cooling passages must be considered in designing the external blade shape. One of the reasons for this is that sufficient internal area must be provided to pass the required amount of cooling air at subcritical velocities and to obviate large pressure drops within the blade. Of even greater significance is the requirement imposed on the external blade shape by the type of internal cooling passages that might be employed to distribute the cooling air over the inner surface of the blade and to act as heat-transfer surfaces.

Since the use of corrugated inserts along the inner surface of the blade was considered as a possible solution to the cooling-air distribution and heat-transfer problems, this particular cooling configuration dictated the use of blade shapes that would not require bending of the corrugated inserts to any great extent in the radial direction.

It was felt that the three-dimensional design procedures based on three design sections which have been used previously (see ref. 2) would result in considerable bending of the corrugated inserts; therefore, a modified three-dimensional design procedure based on the design of only two blade sections was developed. By designing only two blade sections and fairing the rest of the blade with straight lines through corresponding points on the two blade sections as discussed in the appendix, the bending of the corrugated inserts is minimized.

In order to have internal blade cooling passages close to the trailing edge, a wedge-shaped trailing edge was used in all four blade rows. The wedge angle at the trailing edge is about 10° for each blade row with about an equal division of the wedge angle between the suction and pressure surfaces. The use of a wedge-shaped trailing edge requires a certain amount of curvature on the suction surface downstream of the channel exit (fig. 3). The effects of curvature along this portion of the suction surface on the blade profile loss and exit flow angle are discussed subsequently in the section entitled Discussion of Blade Design Procedure.

Considerations of Two-Section Blade Design Procedure

As previously pointed out, a fairly straight blade shape is desired in order that corrugated inserts, if used, would not be bent to any great degree in the radial direction. In order to do this a blade design based on only two sections instead of the usual three or more was adopted. The two design sections chosen were sections B and D of figure 4(a). Section B corresponds to a radius equal to the mean-section radius plus one-fourth

the blade height at the blade trailing edge, and section D corresponds to a radius equal to the mean-section radius minus one-fourth the blade height at the blade trailing edge. It should be noted that the radius of section B and the radius of section D are constant from the inlet to the outlet of a given blade row, but these radii vary from blade row to blade row. The radius of the mean section (section C) is constant throughout the turbine, as shown in figure 2(a), and the slopes of the inner and outer walls are assumed to be equal and opposite from the inlet to the outlet of a blade row. Small changes in the inner and outer wall contours from those shown in figure 2(a) are shown in figures 2(b) to (d). These progressive design changes and their effects on the design are discussed subsequently.

Since section B is approximately halfway between the mean and tip over the entire axial length of the blade, the surface velocities of section B should be fairly representative of those along the surfaces of the mean and the tip. A similar assumption is made for section D with respect to the hub and mean. Thus, it is assumed that the control of the velocity distributions at sections B and D should be adequate enough to ensure a low blade profile loss. On the basis of this assumption, a design procedure is outlined herein which is based on only two sections. From these two sections three other sections (sections A, C, and E in fig. 4(a)) parallel to the axis of rotation are obtained for blade fabrication purposes by the method given in the appendix.

Design Assumptions

The three-dimensional design procedure used herein is an adaptation of the design procedure given in reference 3 with the modifications discussed in reference 4. The assumptions used in this design procedure consist of the design assumptions given in references 3 and 4, the assumptions made to adapt the two-section blade design to the three-section blade design procedure of reference 3, and the assumptions regarding the cooling air. These assumptions are:

(A) Free-vortex flow exists at all free-stream stations.

(B) Total temperature and total pressure are uniform from hub to tip at all free-stream stations.

(C) Simple radial equilibrium exists in the radial-axial plane from hub to tip at all axial stations. Within the guided channel simple radial equilibrium is assumed to exist from hub to tip along the centerline of a given orthogonal surface.

(D) There is no change in total-state conditions from a free-stream station to a station just inside the trailing edge.

(E) There is no change in the tangential velocity from the free-stream stations to corresponding stations just inside the trailing edge.

(F) In the design of that portion of each blade surface between the inlet and the exit of the guided channel, the relative total pressure is assumed to vary linearly in the axial direction from the leading edge to the trailing edge of the blade.

(G) In order to adapt the two-section design to a three-section design for the purpose of integrating the weight flow crossing a given orthogonal surface, the following quantities are assumed to vary linearly from hub to tip:

(1) The angles β_s and β_p (fig. 5) measured between the suction and pressure surfaces and lines parallel to the axis of rotation at either end of a cross-channel orthogonal

(2) The suction-surface to midchannel velocity ratio and the pressure-surface to midchannel velocity ratio

(3) The cross-channel orthogonal length (fig. 5)

(H) The addition of turbine cooling air to the mainstream flow is assumed to be linear in the axial direction from the leading edge to the trailing edge of a blade row.

(I) As soon as any portion of the cooling air enters the main stream within a given blade row, the total-state and flow conditions of the cooling air are the same as those of the main stream. To this extent the cooling air is considered to be a blockage uniformly distributed over the channel at a particular axial station. As pointed out in reference 1, in either a cold-air test of the turbine or in a test of an actual engine at design operating conditions, the total temperature and total pressure of the cooling air would probably not be too far different from those of the mainstream flow. Therefore, this assumption is considered to be reasonable.

Assumption (I) indicates that the cooling air is assumed to produce some work in following a streamline path similar to that of the mainstream flow, but it would be difficult to incorporate this work in the calculation of the stage work outputs. Therefore, the cooling air is neglected in calculating the work of each stage, but it is accounted for in considering the cooling air as a free-stream flow blockage.

Trailing-Edge Thickness, Solidity, and Design Velocity Diagrams

As pointed out in reference 5, the over-all blade loss decreases with a decrease in the trailing-edge thickness; therefore, it was desired

to have a thin trailing edge. However, in order that the internal blade cooling passages could come sufficiently close to the trailing edge to adequately cool the trailing-edge region, the trailing-edge thickness was limited to a minimum of 0.030 inch for all four blade rows.

The free-stream velocity diagrams at the hub, mean, and tip shown in figure 1 for the inner and outer wall configurations of figure 2(a) are used as the basis for calculating the design velocity diagrams at the design sections. Since the blades were designed using sections B and D (fig. 4(a)), as previously discussed, it was necessary to calculate the free-stream velocity diagrams for these two sections (fig. 6) on the basis of assumptions (A) to (C). In the design of a blade section, however, the trailing-edge design was based on the velocity diagram calculated for the station just inside the trailing edge on the basis of assumptions (D) and (E) and continuity, considering the effect of trailing-edge blockage only. In order to calculate the trailing-edge blockage, it is necessary to determine the pitch, or spacing, of the blades in addition to the prescribed trailing-edge thickness.

In determining the pitch of the blades two things were considered, namely, the solidity and the axial chord length. For each blade row a value of solidity was chosen that would result in a satisfactory velocity distribution from the standpoint of low surface diffusions. If later in the design procedure it was found that the velocity distribution was unsatisfactory, the solidity was changed as required. In the over-all engine design it was proposed that the turbine rotor shaft would be cantilevered from a bearing located at an axial position approximately equal to that of the leading edge of the first-stage stator. For this reason, an effort was made to reduce the axial length of the turbine by reducing the axial chord length of each blade row as much as possible without causing the blade to be so thin that it would be impossible to install internal blade cooling passages.

For the selected values of solidity and the selected wedge angle of 10°, preliminary blade sections and channels were drawn for all four blade rows. These sections were analyzed to determine the extent to which the blade section could be scaled down and still provide adequate internal cooling area. By this method the final axial chord lengths of the first-stage stator and rotor and the second-stage stator and rotor were determined to be 1.8, 2.5, 2.0, and 2.5 inches, respectively. This variation in axial chord length of the last three blade rows results in the inner and outer wall configuration shown in figure 2(b).

For these values of axial chord length and solidity, the pitch of each blade section can also be determined. Then the trailing-edge blockage δ_{te} can be calculated by the equation

[redacted]

$$\delta_{te} = \frac{t}{s \cos \beta}$$

where β is the free-stream flow angle, which is approximately equal to the flow angle just inside the trailing edge. Then, on the basis of continuity, the weight-flow parameter at the station just inside the trailing edge was calculated by the equation

$$\left(\frac{\rho W_x}{\rho'' W_{cr}}\right)_a = \left(\frac{1}{1 - \delta_{te}}\right)\left(\frac{\rho W_x}{\rho'' W_{cr}}\right)$$

With this weight-flow parameter inside the trailing edge and the tangential critical velocity ratio from assumption (E), the velocity diagram inside the trailing edge was determined by use of the "flow chart" shown in figure 3 of reference 6. The velocity diagrams for each station just inside the trailing edge are shown in figure 6.

BLADE DESIGN PROCEDURE

During the blade design there were progressive changes of the turbine inner and outer walls as indicated in figure 2. In reference 1 velocity diagrams were evolved for the configuration shown in figure 2(a), which has equally spaced free-stream stations and equally divergent inner and outer walls from stations 1 to 4. In order to shorten the turbine for the mechanical reasons previously mentioned, the axial chord length of each blade row was shortened as much as possible, resulting in axial chord lengths of 2.5 inches for the first- and second-stage rotors and 2.0 inches for the second-stage stator. This difference in the axial chord lengths between the rotors and the second-stage stator then resulted in the configuration shown in figure 2(b). To allow sufficient clearance between the blade rows for the instrumentation to be used and the manufacturing tolerances specified, the blade rows were spaced 5/8 inch apart as shown in figure 2(c). Then, in order to provide straight inner and outer walls, straight lines were drawn at the hub and tip from station 1 to station 4 as shown in figure 2(d). In the final manufacturing drawing, the hub radius at the inlet of each of the last three blade rows was reduced by 0.015 inch to prevent the mainstream flow from impinging on a sharp corner in case of expansion of either the rotor shaft or the outer casing to which the stator blades are fastened. To define the wall at the hub, a straight line was drawn from the new leading edge of the blade base to the blade hub outlet radius. This last change is insignificant insofar as the turbine aerodynamics is concerned, and it is neglected hereafter.

In the blade profile design the suction surface is divided into three parts, namely, that portion upstream of the channel inlet (fig. 3), that portion downstream of the channel exit, and that portion between the

inlet and exit of the guided channel. In the design procedure the two portions of the suction surface outside the guided channel are designed on the basis of the angles given in the design velocity diagrams of figure 6, consideration being given to the divergence of the inner and outer walls as shown in figure 2(d) in establishing the length of the channel exit l_{ce} (fig. 3(a)). The third portion of the suction surface and the entire length of the pressure surface between the inlet and outlet of the guided channel were designed using a three-dimensional channel design procedure similar to those used in references 3 and 4. For the design of the guided channel, the inner and outer wall configuration of figure 2(c) was used in order that the channel design would be consistent with the design velocity diagrams used.

In the following outline of the design procedure, that portion of the procedure concerned with the design of the guided channel can be divided into a preliminary surface velocity investigation to detect unacceptable velocity fluctuations along the blade surface, an iteration process of matching an assumed surface velocity distribution with the design weight flow, elimination of large surface diffusions by alterations of the channel design, and a repetition of the iteration process mentioned, if necessary.

The detailed blade design procedure is given in the following steps:

(1) The trailing edges of two adjacent blades were represented by circles of 0.030-inch diameter drawn 1 blade pitch apart.

(2) To represent the suction surface at the trailing edge, a line was drawn tangent to one circle at an angle 5° larger than the flow angle inside the trailing edge β_a (fig. 3).

(3) To represent the pressure surface at the trailing edge, a line was drawn tangent to the other circle at an angle 5° smaller than β_a. (The lines drawn in steps (2) and (3) then represent a 10° wedge angle at the trailing edge.)

(4) Assuming that the channel exit area over the blade height should be equal to the annulus area at the blade exit minus the trailing-edge blockage, the length of the channel exit at each of the two design sections of each of the last three blade rows was adjusted to compensate for the change in annulus area from station 1 to station 4 on the basis of the inner and outer wall divergence shown in figure 2(d). The method of determining the length of the channel exit is as follows:

[redacted]

(a) The approximate axial distance from the trailing edge to the center of the channel exit was calculated by the equation

$$d = \frac{1}{2}\left(s - \frac{t}{\cos \beta_a}\right) \cos(\beta_a - \psi) \sin(\beta_a - \psi)$$

where ψ is half the wedge angle.

(b) The constant and equal slopes of the inner and outer walls from stations 1 to 4 (fig. 2(d)) were determined from the change in the radius of both the inner and outer walls between these two stations. In reference 1 the hub radius was specified to change from 9.555 to 8.555 inches between stations 1 and 4, and the tip radius was specified to change from 14.000 to 15.000 inches over the same distance. In the final design of the turbine the clearance between blade rows is specified to be about 5/8 inch; therefore, the axial length of the turbine from the outlet of the first-stage stator to the outlet of the second-stage rotor is $8\frac{7}{8}$ inches. From these values, the slopes m_t and m_h of the inner and outer walls were calculated. (Note that the two slopes are equal in magnitude but opposite in sign.)

(c) Using the values of d, m_t, and m_h calculated in steps (4a) and (4b), the blade height at the center of the channel exit b_c was calculated by the equation

$$b_c = (r_{t,a} - m_t d) - (r_{h,a} - m_h d)$$

$$= r_{t,a} - r_{h,a} - (m_t - m_h)d$$

Since $m_t = -m_h$, then

$$b_c = r_{t,a} - r_{h,a} - 2m_t d$$

(d) The length of the channel exit was then calculated from the ratio of blade height at the trailing edge to the blade height at the center of the channel exit by the equation

$$l_{ce} = \left(s - \frac{t}{\cos \beta_a}\right) \cos(\beta_a - \psi) \frac{b_a}{b_c} \qquad (1)$$

(5) As shown in figure 3, the channel exit was located on a line that was drawn perpendicular to the line drawn in step (3) at the point

of tangency of the line of step (3) and the trailing-edge circle. The length of the channel exit calculated in step (4d) was then measured along this line.

(6) At the suction-surface end of the channel exit a line was drawn perpendicular to the channel exit.

(7) Having thus determined two lines tangent to the suction surface as well as their points of tangency in steps (2) and (6), a drafting spline was located tangent to these two lines at the specified points of tangency. A brief examination of the shape of the resulting portion of the suction surface downstream of the channel exit was then made to determine whether or not the local curvatures were excessive. If the local curvatures were excessive, an attempt was made to distribute more evenly the curvature along this portion of the suction surface either by reducing the wedge angle or by changing its position slightly with subsequent changes in the channel exit position.

(8) At the leading edge of each blade row the suction and pressure surfaces were drawn to converge to a point termed the design leading edge (fig. 3). The axial location of the design leading edge corresponded to an axial distance forward of the trailing edge equal to the axial chord length previously specified for each blade row plus an additional length estimated on the basis of the type of wedge shape desired at the leading edge. The tangential location of the leading edge with respect to the trailing edge (described by length a in fig. 3) was determined by locating the design leading edge in such a way that good curvature distribution was obtained on the suction surface between the inlet and exit of the guided channel. The design of the leading edge of the stators differs from that of the rotors as follows:

(a) At the design leading edge of each of the stators the suction and pressure surfaces were made to converge at an angle of about 20° to 30° with each other and to have about equal but opposite incidence angles with the mainstream flow. Therefore, the resulting design axial chord lengths were about 0.1 inch longer than the specified axial chord length of the final blade shape with a rounded leading edge.

(b) At the design leading edge of the rotors the pressure surface was drawn tangent to the suction surface (fig. 3(b)), and at this point the angle of both surfaces was equal to that of the blade inlet free-stream flow. With this type of leading-edge design the blade is usually sufficiently thick with respect to turbine cooling to round off the leading edge at an axial distance of about 1/2 inch from the design leading edge. Therefore, the design axial chord length of the rotors was specified to be 3.0 inches. From the design leading edge to the design channel inlet the suction surface was represented by a straight line at an angle equal to the inlet free-stream relative flow angle (see fig. 3(b)).

[redacted]

(9) A suction surface was then represented by an arbitrary curve connecting the portion of the suction surface upstream of the channel inlet with that downstream of the channel exit. Local curvatures on the suction surface were measured with a curvometer described in appendix B of reference 4. Large local curvatures were reduced by changing the distribution of the curvature from channel inlet to channel outlet, by changing the tangential position of the leading edge relative to the trailing edge, or by changing the position or amount of the wedge angle at the trailing edge.

4236

(10) The pressure surface was then represented by an arbitrary curve drawn from the design leading edge to the point of tangency at the trailing-edge circle determined in step (3).

(11) A series of orthogonal lines (fig. 5) was drawn from the suction surface to the pressure surface. At the ends of these orthogonal lines the local curvatures of the suction and pressure surfaces were measured by a curvometer. The lengths of the orthogonal lines were also measured.

(12) Using the values obtained in step (11), the ratio of the suction-surface velocity to the midchannel velocity W_s/W_{mid} and the ratio of the pressure-surface velocity to the midchannel velocity W_p/W_{mid} were calculated at each orthogonal line by equations (39) and (40) of reference 7, which in the symbols of this report are as follows:

$$\frac{W_s}{W_{mid}} = \exp\left[\frac{C_s l_o}{2}\left(1 - \frac{C_s - C_p}{4C_s}\right)\right] \tag{2}$$

$$\frac{W_p}{W_{mid}} = \exp\left\{-\frac{C_s l_o}{2}\left[1 - \frac{3(C_s - C_p)}{4C_s}\right]\right\} \tag{3}$$

(13) In order to detect undesirable surface velocity fluctuations resulting from a combination of local surface curvatures and orthogonal lengths as represented in equations (2) and (3), a preliminary surface velocity check was made without considering the continuity requirements. This was done by assuming a suction-surface velocity distribution that would satisfy the surface diffusion requirements and then calculating the midchannel and pressure-surface velocity distribution by equations (2) and (3). If the midchannel and/or the pressure-surface velocities had large local fluctuations, the blade profile was changed in order to give a steadier velocity variation, and steps (9) to (13) were repeated.

(14) Having established the channel design for both sections B and D of a given blade row in the preceding steps, sections B and D of the stators were stacked so that the centers of the channel exits (fig. 3(a))

were in a common radial plane perpendicular to the axis of rotation, and sections B and D of the rotors were stacked so that their trailing edges would be tangent to a common radial plane perpendicular to the axis of rotation. Then, assumptions (G1) to (G3) were used to estimate the quantities β_{av}, W_s/W_{mid}, W_p/W_{mid}, and l_o at the hub, mean, and tip radii.

(15) From the values of β_{av} obtained in step (14) at the hub, mean, and tip, the ratio of the midchannel velocity at the hub or the tip to that at the mean was obtained from equation (3) of reference 8, which is based on simple radial equilibrium. A rearranged form of this equation with the symbols of this report is

$$\frac{W_{mid,r}}{W_{mid,r_m}} = \left(1 - \frac{\int_{r_m}^{r} ke^{-\int_{r_m}^{r} j\,dr}\,dr}{W_{mid,r_m}} \right) e^{\int_{r_m}^{r} j\,dr} \tag{4}$$

where

$$j = -\frac{\sin^2\beta_{av}}{r}$$

$$k = 2\omega \sin \beta_{av}$$

(16) By assuming a midchannel velocity distribution at the mean section, the midchannel velocity distributions at the hub and tip were calculated by using the ratios $W_{mid,h}/W_{mid,m}$ and $W_{mid,t}/W_{mid,m}$ obtained in step (15). Then, with the ratios W_s/W_{mid} and W_p/W_{mid} calculated in step (12), the suction- and pressure-surface relative velocity ratios, W_s/W_{cr} and W_p/W_{cr}, respectively, were calculated at the hub, mean, and tip.

(17) With the values of l_o, W_s/W_{cr}, and W_p/W_{cr} obtained, the average integrated mass flow across each selected orthogonal surface was calculated by the following equation:

$$w = N \int_{r_h}^{r_t} \int_{0}^{l_o} \rho W \, dl \, dr$$

In the integration of ρW along the orthogonal a linear variation in static pressure from the suction surface to the pressure surface was assumed, and the tables for a ratio of specific heats of 1.3 and the method of integration of reference 9 were used.

(18) On the basis of assumption (H), the design weight flow crossing each orthogonal surface was calculated. These values were compared with those obtained in step (17). If the weight flows of step (17) differed from the design values by more than 1 percent at corresponding axial stations, then the original assumption of the midchannel velocity distribution at the mean of step (16) was altered until the calculated and design weight flows agreed within 1 percent.

(19) From the final midchannel velocity distribution at the mean obtained in step (18), the midchannel velocities at sections B and D were obtained by using equation (4).

(20) The suction- and pressure-surface velocity distributions of sections B and D were then calculated from the midchannel velocities calculated in step (19) and the ratios W_s/W_{mid} and W_p/W_{mid} determined in step (12).

(21) Since all four blade rows were designed with a curved suction surface downstream of the channel exit, some suction-surface diffusion would have to be accepted. Within the channel the upper limits of the suction-surface diffusion parameter D_s, which is a measure of the suction-surface diffusion, were set at 0.15 for the stators and 0.20 for the rotors. If any of the calculated suction-surface diffusion parameters at sections B and D exceeded these limits, then the blade channel was redesigned with changes to reduce the suction-surface diffusion parameter.

Final Blade Shapes

From the design sections B and D, three other sections (A, C, and E, fig. 4(a)) were obtained by the method outlined in the appendix. These five blade profiles were then stacked in the manner discussed in the appendix.

The final blade channels and profiles for sections B and D for all four blade rows are shown in figure 7. The coordinates for the five blade sections of all four blade rows are given in table I. The typical profiles for use in reading the table are given in figures 4(b) and (c).

Discussion of Blade Design Procedure

The design of a three-dimensional blade row is usually based on at least three blade sections that adequately define the necessary channel

quantities required at the hub, mean, and tip. However, for the type of air-cooled blade proposed for the subject application, a fairly straight blade was required. Since a three-section design might possibly have resulted in undesirable bending of the blade internal cooling passages, the blades for the subject turbine were based on only two sections (B and D, fig. 4(a)). On the basis of a linear variation in the radial direction of the four design quantities β_{av}, l_o, W_s/W_{mid}, and W_p/W_{mid} based on the values at the two design sections B and D, the values of these four quantities were obtained at the hub, mean, and tip. It should be noted that the four quantities thus obtained do not represent the actual values for the final blade shapes at the hub, mean, and tip obtained from sections B and D by the method of the appendix and the subsequent conformation to the inner and outer walls shown in figure 2(d). The calculated values of these four quantities represent only good approximations of those that actually exist in the final design.

In order to compare the design method based on two sections with that based on three sections, the weight flows obtained by the two different methods were compared. The blade used for this comparison had been designed previously using three design sections. The differences between the weight flows calculated by the two different methods was less than 1 percent for the same midchannel velocity distribution at the mean. This means then that the velocity distributions for sections B and D for each of the blade rows designed herein should be fairly representative of those that would have been obtained by a three-section design method.

In the design of all four blade rows the inner and outer wall configuration shown in figure 2(c) was assumed, but subsequently the inner and outer wall configurations for the last three blade rows were changed to those shown in figure 2(d). As indicated in figure 2(d), the hub and tip radii of the final inner and outer wall configuration are slightly different from the corresponding radii indicated in figure 2(c). At the leading edges of the first-stage rotor, the second-stage stator, and the second-stage rotor, the differences in the annular area between the two configurations are 3.2, 3.5, and 1.8 percent, respectively. For the first-stage rotor this represents an increase in the relative inlet flow angle of 1.1° and a decrease in the relative critical velocity ratio of about 2 percent. It should be noted that the hub and tip radii at the trailing edge of the second-stage rotor were not changed, and at the trailing edge of the first-stage rotor and the second-stage stator the changes in the hub and tip radii changed their respective annular areas by less than 0.8 percent. Therefore, the flow angles and velocities at the trailing edges of the latter two blade rows would be changed by a negligible amount.

In reference 10 a relation between the blade profile loss and the suction-surface curvature downstream of the channel exit is presented on

the basis of cascade data obtained at turbulence levels below those usually encountered in turbines. The variation in the profile loss is therein presented over a range of Mach numbers as a function of a ratio of the blade spacing to the average radius of curvature of that portion of the suction surface downstream of the channel exit s/r_c. In order to predict the magnitude of the losses attributed to this suction-surface curvature, the value of s/r_c was approximated by the equation

$$\frac{s}{r_c} = \frac{s}{\frac{s \sin \beta}{2\psi \left(\frac{\pi}{180^\circ}\right)}} = \frac{\pi\psi}{90^\circ \sin \beta} \tag{5}$$

where $s \sin \beta$ approximates the length of the suction surface downstream of the channel exit, and where 2ψ represents the angle through which the suction surface turns downstream of the channel exit. The values of $s \sin \beta$ and 2ψ then approximate an arc length and an arc angle, respectively, from which a radius of curvature r_c can be obtained. The largest value of s/r_c would then correspond to the blade section with the smallest exit flow angle, which according to figure 1 is the second-stage rotor hub. This section has a relative exit flow angle of $40^\circ 17'$, and the corresponding value of s/r_c would then be 0.27. From figure 12(a) of reference 10 the additional profile loss would be approximately 10 percent of the blade profile loss for a straight-backed blade. The magnitude of the additional losses attributed to the curvature on the suction surface downstream of the channel exit is considered to be very questionable, because the turbulence level in the second-stage rotor is considered to be much higher than that of the cascade used to determine the results presented in figure 12(a) of reference 10.

The curvature of the suction surface downstream of the channel exit also has an effect on the blade outlet flow angle, as discussed in reference 10, which gives a relation between the value of s/r_c and the change in the outlet flow angle. Since the blade exit Mach numbers of the subject turbine are in the high subsonic Mach number range, the values obtained from using figure 12(b) of reference 10 based on a blade exit Mach number of 1.0 should be of the right magnitude. Using values of s/r_c calculated by equation (5) and approximations of the flow angle at the channel exit, it was found that for most of the blade sections the curvature of the suction surface downstream of the channel exit would affect the exit flow angle by less than 0.5° and in all cases by less than 1.0°.

DISCUSSION OF DESIGN RESULTS

The design values of the mean-section solidity and the number of blades for each row are listed in table II. Of the four blade rows, the turning in the first-stage rotor is the largest; and table II shows that in the final design this blade row has the highest solidity. From the surface velocity distributions shown in figures 8(c) and (d), it can be shown that a somewhat lower solidity could have been used without exceeding the surface diffusion values of figures 8(c) and (d). However, the redesign would not have resulted in a major improvement; therefore, the first-stage rotor design was not changed.

It should also be noted that the solidity of 1.927 for the second-stage stator is also high. This high solidity occurred because, as in the first-stage rotor, there is a large inlet tangential velocity. Therefore, a higher solidity than those usually associated with stators was required for the second-stage stator to avoid large surface diffusions.

From the surface velocity distribution for sections B and D in figure 8, it can be seen that all four blade rows have a certain amount of suction-surface diffusion. Based on an average of values at sections B and D, the second-stage rotor has the highest value of the suction-surface diffusion parameter, 0.151 (table II). A diffusion of this magnitude is not considered excessive (ref. 4). The other blade rows had average suction-surface diffusion parameters of less than 0.100.

CONCLUDING REMARKS

A blade design study was made for a two-stage air-cooled turbine suitable for flight at a Mach number of 2.5 for which velocity diagrams had been previously obtained. The detailed procedure used in the design of the blades was given. In addition, the design blade shapes, surface velocity distributions, inner and outer wall contours, and other design data were presented. The important results of the design are as follows:

1. The first-stage rotor had the highest solidity, with a value of 2.289 at the mean section.

2. The second-stage stator also had a high mean-section solidity of 1.927, mainly because of its high inlet whirl.

3. The second-stage rotor has the highest suction-surface diffusion parameter, with a value of 0.151. All other blade rows have values under 0.100.

Lewis Flight Propulsion Laboratory
National Advisory Committee for Aeronautics
Cleveland, Ohio, November 8, 1956

[redacted]

APPENDIX - METHOD OF DETERMINING BLADE SHAPES AT HUB, MEAN, AND TIP FROM TWO INTERMEDIATE SECTIONS

In the design procedure of this report, blade sections B and D (fig. 4(a)) were determined. In order to adequately define the blade shape for fabrication, it was also necessary to determine sections A, C, and E (fig. 4(a)). For all four blade rows the method of fairing is the same, but the way in which sections B and D are located with respect to each other is different for the stators and rotors; therefore, they are discussed separately.

Stator Blade Sections

For the stator blades the method of determining sections A, C, and E from the design sections B and D is as follows:

(1) The suction surface of section B was divided into equal segments and the end points of the segments were numbered from the leading edge. The pressure surface was similarly divided into equal segments. Then the profile of section D was divided in the same manner with the number of segments on each surface corresponding to those of section B.

(2) Assuming that sections B and D were flat instead of sections on a cylindrical surface, the radial distances between sections A, B, C, D, and E were determined from the radii of the sections.

(3) The two design sections B and D were placed one over the other so that the center of the channel exit of adjacent blades at section B was directly over the center of the channel exit of adjacent blades at section D and so that each blade profile was oriented at the proper blade stagger angle.

(4) Straight lines were drawn through corresponding points on the suction and pressure surfaces of sections B and D. Corresponding points on section C were obtained by bisecting each line between points on sections B and D. Corresponding points on section A were obtained by measuring along each straight line between points on sections B and D a distance equal to the horizontal distance between points on sections B and D multiplied by the ratio of the radial distance between sections A and B to that between sections B and D. Points on section E were obtained in a manner similar to those on section A.

(5) The profiles of sections A, C, and E were then determined by fairing curves through the points obtained for these sections in step (4). The rounded leading and trailing edges were defined by arcs of circles drawn tangent to the suction and pressure surfaces and located

in such a way that in a side view of the blade the leading and trailing edges would be represented by straight lines drawn through corresponding points on sections B and D.

Rotor Blade Sections

The method of determining sections A, C, and E for the rotor blades is largely the same as that for the stator blades, with some exceptions:

(1) and (2) same as steps (1) and (2) for the stator blades.

(3) The center of gravity of sections B and D were determined. Then sections B and D were placed one above the other so that the trailing edges were tangent to the same radial plane perpendicular to the axis of rotation and so that the center of gravity of each section was over the axis of rotation.

(4) and (5) same as steps (4) and (5) for the stator blades.

(6) Cooling-air-passage areas were determined for each section, and then air-passage contours in the radial direction were established. The centers of gravity for the blade profiles with cooling-air-passage areas were calculated, and from these centers of gravity the center of gravity of the entire blade was determined. The center of gravity of section E was located in a radial-axial plane, and then the blade was tilted in the tangential direction so that the center of gravity of the entire blade was located in this same radial-axial plane.

REFERENCES

1. Miser, James W., and Stewart, Warner L.: Investigation of Two-Stage Air-Cooled Turbine Suitable for Flight at Mach Number of 2.5. I - Velocity-Diagram Study. NACA RM E56H14, 1956.

2. Miser, James W., Stewart, Warner L., and Wong, Robert Y.: Effect of a Reduction in Stator Solidity on Performance of a Transonic Turbine. NACA RM E55L09a, 1956.

3. Stewart, Warner L., Wong, Robert Y., and Evans, David G.: Design and Experimental Investigation of Transonic Turbine with Slight Negative Reaction Across Rotor Hub. NACA RM E53L29a, 1954.

4. Miser, James W., Stewart, Warner L., and Monroe, Daniel E.: Effect of High Rotor Pressure-Surface Diffusion on Performance of a Transonic Turbine. NACA RM E55H29a, 1955.

5. Miser, James W., Stewart, Warner L., and Whitney, Warren J.: Analysis of Turbomachine Viscous Losses Affected by Changes in Blade Geometry. NACA RM E56F21, 1956.

6. Alpert, Sumner, and Litrenta, Rose M.: Construction and Use of Charts in Design Studies of Gas Turbines. NACA TN 2402, 1951.

7. Huppert, M. C., and MacGregor, Charles: Comparison Between Predicted and Observed Performance of Gas-Turbine Stator Blade Designed for Free-Vortex Flow. NACA TN 1810, 1949.

8. Stewart, Warner L.: Analytical Investigation of Flow Through High-Speed Mixed-Flow Turbine. NACA RM E51H06, 1951.

9. Whitney, Warren J.: Tabulation of Mass-Flow Parameters for Use in Design of Turbomachine Blade Rows for Ratios of Specific Heats of 1.3 and 1.4. NACA TN 3831, 1956.

10. Ainley, D. G., and Mathieson, G. C. R.: An Examination of the Flow and Pressure Losses in Blade Rows of Axial Flow Turbines. Rep. No. R.86, British N.G.T.E., Mar. 1951.

TABLE I. - BLADE-SECTION COORDINATES

(a) First-stage stator

	Section (fig. 4(a))									
	A		B		C		D		E	
	Radius of section, in.									
	13.851		12.888		11.777		10.666		9.635	
	Stagger angle, α_s, deg									
	45.23		45.23		45.23		45.23		45.23	
X, in.	Y_s, in.	Y_p, in.	Y_s, in.	Y_p, in.	Y_s, in.	Y_p, in.	Y_s, in.	Y_p, in.	Y_s, in.	Y_p, in.
0	0.050	0.050	0.050	0.050	0.050	0.050	0.050	0.050	0.050	0.050
.1	.263	.026	.263	.025	.250	.024	.252	.022	.247	.021
.2	.384	.097	.383	.091	.378	.086	.377	.082	.378	.076
.3	.462	.153	.463	.147	.465	.138	.465	.130	.470	.125
.4	.514	.196	.519	.189	.526	.180	.531	.171	.538	.164
.5	.548	.229	.557	.223	.566	.213	.576	.203	.587	.196
.6	.568	.253	.579	.246	.592	.237	.605	.228	.619	.223
.7	.574	.266	.589	.259	.603	.253	.621	.247	.638	.242
.8	.569	.272	.587	.267	.602	.262	.623	.258	.643	.258
.9	.555	.270	.575	.268	.594	.266	.615	.265	.635	.268
1.0	.537	.262	.557	.263	.578	.265	.599	.268	.617	.273
1.1	.515	.250	.536	.255	.556	.260	.575	.265	.593	.272
1.2	.491	.237	.511	.244	.530	.252	.547	.258	.562	.267
1.3	.465	.223	.485	.231	.501	.239	.516	.248	.527	.257
1.4	.439	.207	.457	.218	.470	.226	.481	.236	.489	.243
1.5	.410	.192	.426	.201	.436	.211	.445	.220	.450	.227
1.6	.382	.174	.394	.185	.400	.194	.407	.201	.408	.206
1.7	.352	.158	.360	.169	.364	.175	.366	.181	.363	.183
1.8	.320	.142	.325	.151	.326	.155	.324	.160	.317	.159
1.9	.287	.124	.289	.133	.286	.135	.280	.137	.269	.134
2.0	.253	.108	.252	.113	.242	.114	.235	.112	.220	.108
2.1	.217	.091	.215	.094	.204	.092	.189	.088	.169	.080
2.2	.182	.072	.177	.075	.161	.070	.142	.063	.118	.052
2.3	.147	.054	.138	.054	.119	.048	.097	.037	.067	.020
2.385	----	----	----	----	----	----	----	----	.015	.015
2.4	.112	.037	.099	.034	.076	.024	.050	.010	----	----
2.452	----	----	----	----	----	----	.015	.015	----	----
2.5	.076	.020	.060	.015	.035	.000	----	----	----	----
2.518	----	----	----	----	.015	.015	----	----	----	----
2.584	----	----	.015	.015	----	----	----	----	----	----
2.6	.040	.003	----	----	----	----	----	----	----	----
2.640	.015	.015	----	----	----	----	----	----	----	----

TABLE I. - Continued. BLADE-SECTION COORDINATES

(b) First-stage rotor

	Section (fig. 4(a))									
	A		B		C		D		E	
	Radius of section, in.									
	14.352		13.055		11.777		10.499		9.203	
	Stagger angle, α_s, deg									
	33.25		23.37		19.00		9.92		-1.00	
X, in.	Y_s, in.	Y_p, in.	Y_s, in.	Y_p, in.	Y_s, in.	Y_p, in.	Y_s, in.	Y_p, in.	Y_s, in.	Y_p, in.
0	0.031	0.031	0.038	0.038	0.045	0.045	0.052	0.052	0.059	0.059
.1	.195	.047	.220	.045	.250	.038	.271	.026	.289	.016
.2	.328	.121	.364	.128	.410	.130	.452	.130	.484	.121
.3	.432	.185	.480	.198	.540	.209	.600	.215	.649	.216
.4	.516	.240	.570	.255	.640	.273	.715	.288	.778	.299
.5	.584	.285	.643	.305	.721	.330	.808	.351	.882	.368
.6	.640	.322	.702	.347	.787	.378	.880	.404	.966	.428
.7	.682	.353	.748	.381	.837	.415	.935	.448	1.031	.478
.8	.716	.379	.780	.409	.872	.446	.975	.483	1.081	.518
.9	.740	.399	.803	.431	.895	.470	1.004	.512	1.117	.552
1.0	.755	.415	.818	.448	.909	.488	1.020	.532	1.140	.578
1.1	.761	.426	.821	.459	.911	.500	1.023	.548	1.151	.596
1.2	.759	.432	.817	.464	.903	.506	1.016	.555	1.150	.608
1.3	.750	.433	.803	.465	.887	.505	1.000	.557	1.138	.612
1.4	.732	.431	.781	.460	.861	.501	.971	.552	1.113	.610
1.5	.710	.423	.752	.450	.829	.490	.932	.540	1.079	.600
1.6	.681	.412	.720	.438	.785	.473	.882	.521	1.028	.582
1.7	.648	.398	.680	.419	.735	.451	.821	.495	.962	.557
1.8	.612	.380	.636	.397	.679	.422	.751	.462	.882	.521
1.9	.573	.359	.589	.370	.618	.390	.672	.420	.792	.476
2.0	.533	.334	.538	.340	.550	.351	.589	.372	.690	.420
2.1	.491	.308	.482	.305	.480	.306	.499	.315	.573	.355
2.2	.448	.278	.426	.268	.407	.256	.400	.250	.450	.274
2.3	.401	.246	.366	.225	.329	.201	.295	.178	.411	.181
2.4	.353	.212	.303	.182	.245	.143	.184	.100	.166	.080
2.495	----	----	----	----	----	----	----	----	.015	.015
2.5	.303	.177	.236	.137	.158	.080	.070	.016	----	----
2.541	----	----	----	----	----	----	.015	.015	----	----
2.6	.250	.140	.167	.089	.065	.015	----	----	----	----
2.643	----	----	----	----	.015	.015	----	----	----	----
2.7	.197	.104	.094	.040	----	----	----	----	----	----
2.796	----	----	.015	.015	----	----	----	----	----	----
2.8	.140	.066	----	----	----	----	----	----	----	----
2.9	.079	.028	----	----	----	----	----	----	----	----
2.992	.015	.015	----	----	----	----	----	----	----	----

[redacted]

TABLE I. - Continued. BLADE-SECTION COORDINATES

(c) Second-stage stator

	Section (fig. 4(a))									
	A		B		C		D		E	
	Radius of section, in.									
	14.647		13.221		11.777		10.333		8.907	
	Stagger angle, α_s, deg									
	25.87		25.65		25.55		25.50		25.42	
X, in.	Y_p, in.	Y_s, in.	Y_p, in.	Y_s, in.	Y_p, in.	Y_s, in.	Y_p, in.	Y_s, in.	Y_p, in.	Y_s, in.
0	0.054	0.054	0.050	0.050	0.048	0.048	0.045	0.045	0.040	0.040
.1	.020	.181	.024	.193	.030	.201	.036	.208	.047	.222
.2	.074	.270	.089	.286	.104	.303	.123	.320	.144	.341
.3	.118	.334	.140	.355	.168	.379	.194	.402	.226	.428
.4	.151	.383	.182	.408	.217	.435	.252	.465	.292	.496
.5	.175	.417	.212	.447	.256	.480	.298	.513	.345	.549
.6	.192	.440	.236	.474	.284	.512	.332	.547	.384	.584
.7	.204	.453	.253	.490	.304	.530	.357	.568	.410	.608
.8	.211	.458	.262	.497	.317	.539	.371	.578	.426	.619
.9	.213	.456	.266	.496	.323	.538	.378	.578	.434	.619
1.0	.211	.446	.265	.487	.322	.528	.377	.569	.432	.610
1.1	.206	.430	.260	.470	.316	.513	.369	.553	.421	.591
1.2	.198	.410	.251	.448	.304	.489	.354	.526	.403	.563
1.3	.189	.385	.237	.421	.287	.460	.333	.494	.377	.525
1.4	.176	.357	.221	.390	.265	.424	.307	.454	.344	.480
1.5	.162	.327	.201	.356	.240	.385	.275	.410	.305	.429
1.6	.146	.296	.179	.319	.212	.342	.238	.360	.260	.374
1.7	.128	.263	.154	.279	.179	.295	.198	.307	.211	.314
1.8	.109	.228	.126	.236	.144	.245	.156	.250	.160	.249
1.9	.086	.189	.098	.191	.107	.192	.111	.190	.106	.180
2.0	.064	.148	.068	.143	.069	.137	.065	.126	.051	.107
2.1	.040	.104	.036	.092	.030	.079	.018	.061	.001	.033
2.113	----	----	----	----	----	----	----	----	.016	.016
2.154	----	----	----	----	----	----	.016	.016	----	----
2.192	----	----	----	----	.016	.016	----	----	----	----
2.20	.015	.058	.003	.040	----	----	----	----	----	----
2.230	----	----	.016	.016	----	----	----	----	----	----
2.268	.016	.016	----	----	----	----	----	----	----	----

[redacted]

TABLE I. - Concluded. BLADE-SECTION COORDINATES

(d) Second-stage rotor

	Section (fig. 4(a))									
	A		B		C		D		E	
	Radius of section, in.									
	15.000		13.388		11.777		10.166		8.555	
	Stagger angle, α_s, deg									
	32.45		26.00		15.43		3.83		-3.83	
X, in.	Y_s, in.	Y_p, in.	Y_s, in.	Y_p, in.	Y_s, in.	Y_p, in.	Y_s, in.	Y_p, in.	Y_s, in.	Y_p, in.
0	0.030	0.030	0.030	0.030	0.030	0.030	0.030	0.030	0.030	0.030
.1	.117	.026	.123	.029	.127	.034	.136	.039	.140	.039
.2	.182	.064	.194	.075	.207	.085	.224	.097	.230	.098
.3	.244	.103	.261	.117	.284	.133	.308	.148	.318	.153
.4	.298	.138	.323	.156	.354	.175	.386	.195	.402	.203
.5	.347	.172	.378	.192	.419	.213	.461	.236	.480	.246
.6	.387	.202	.423	.223	.473	.246	.527	.273	.556	.287
.7	.419	.228	.459	.249	.517	.273	.585	.304	.625	.324
.8	.443	.250	.484	.270	.551	.296	.631	.329	.686	.354
.9	.457	.267	.500	.286	.573	.313	.667	.349	.737	.380
1.0	.465	.279	.507	.296	.585	.324	.691	.364	.778	.400
1.1	.466	.286	.508	.304	.591	.332	.704	.375	.808	.414
1.2	.459	.291	.502	.306	.587	.336	.707	.379	.825	.423
1.3	.448	.292	.488	.304	.574	.334	.698	.379	.830	.427
1.4	.432	.289	.470	.299	.555	.326	.679	.373	.823	.427
1.5	.413	.283	.448	.290	.528	.314	.650	.362	.806	.420
1.6	.392	.273	.424	.276	.496	.298	.612	.344	.775	.407
1.7	.370	.260	.396	.260	.461	.279	.566	.322	.732	.387
1.8	.347	.244	.370	.239	.420	.255	.511	.295	.676	.361
1.9	.324	.224	.340	.216	.373	.227	.451	.262	.607	.330
2.0	.297	.204	.305	.191	.323	.195	.384	.225	.528	.292
2.1	.271	.183	.267	.165	.269	.160	.312	.181	.441	.246
2.2	.243	.161	.227	.137	.211	.122	.236	.134	.350	.195
2.3	.213	.137	.184	.106	.151	.081	.155	.080	.250	.135
2.4	.182	.114	.139	.074	.088	.036	.070	.022	.146	.067
2.455	----	----	----	----	----	----	.015	.015	----	----
2.498	----	----	----	----	.015	.015	----	----	----	----
2.5	.147	.087	.090	.040	----	----	----	----	.034	.001
2.512	----	----	----	----	----	----	----	----	.015	.015
2.6	.115	.062	.041	.004	----	----	----	----	----	----
2.633	----	----	.015	.015	----	----	----	----	----	----
2.7	.080	.036	----	----	----	----	----	----	----	----
2.8	.045	.009	----	----	----	----	----	----	----	----
2.848	.015	.015	----	----	----	----	----	----	----	----

[redacted]

TABLE II. - SUMMARY OF BLADE DESIGN QUANTITIES

	First stage		Second stage	
	Stator	Rotor	Stator	Rotor
Number of blades	41	64	65	50
Solidity at mean section, σ_m	1.395	2.289	1.927	1.687
Average suction-surface diffusion parameter, D_s	0.090	0.096	0.082	0.151
Average pressure-surface diffusion parameter, D_p	0.639	0.325	0.402	0.316

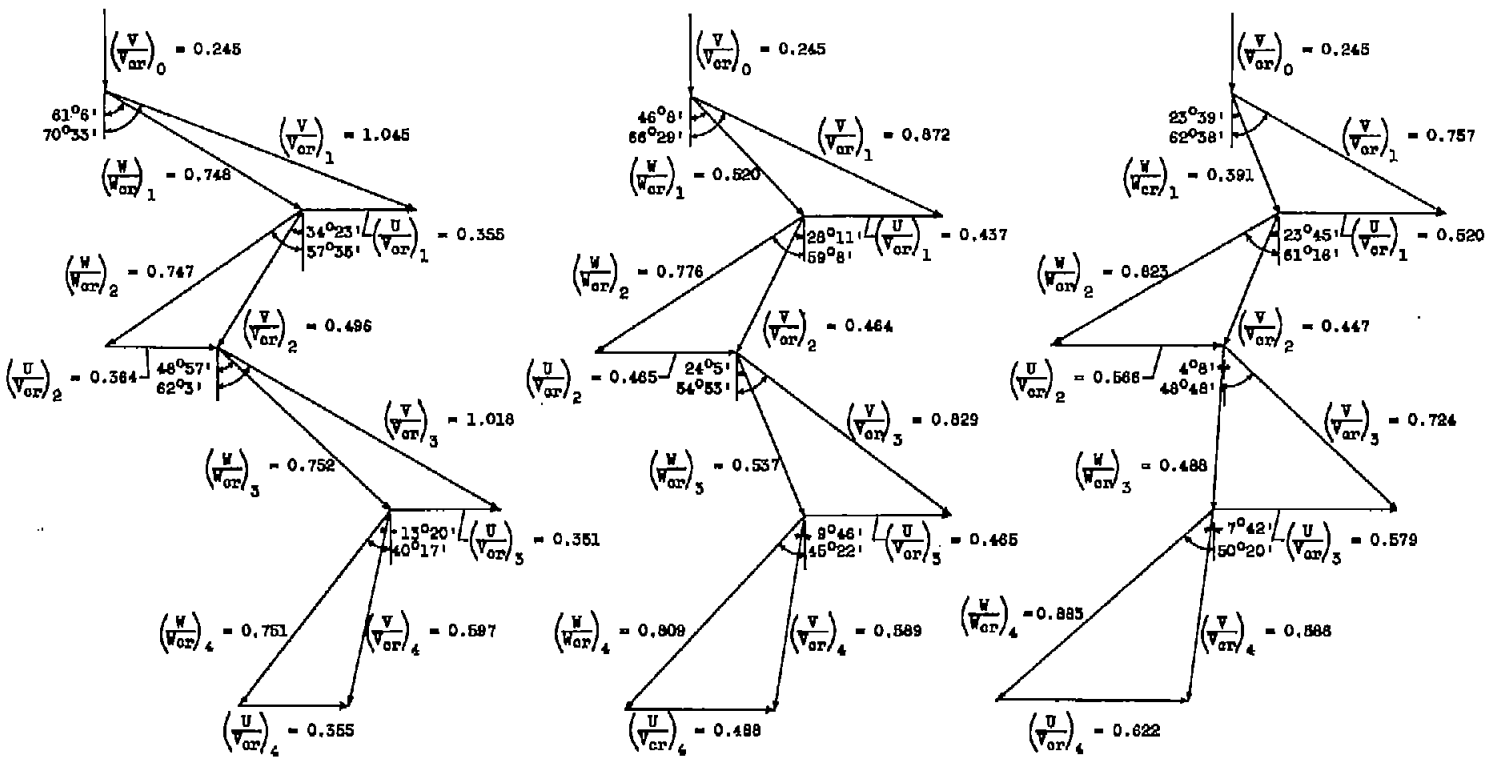

Figure 1. - Velocity diagram for two-stage turbine configuration of reference 1.

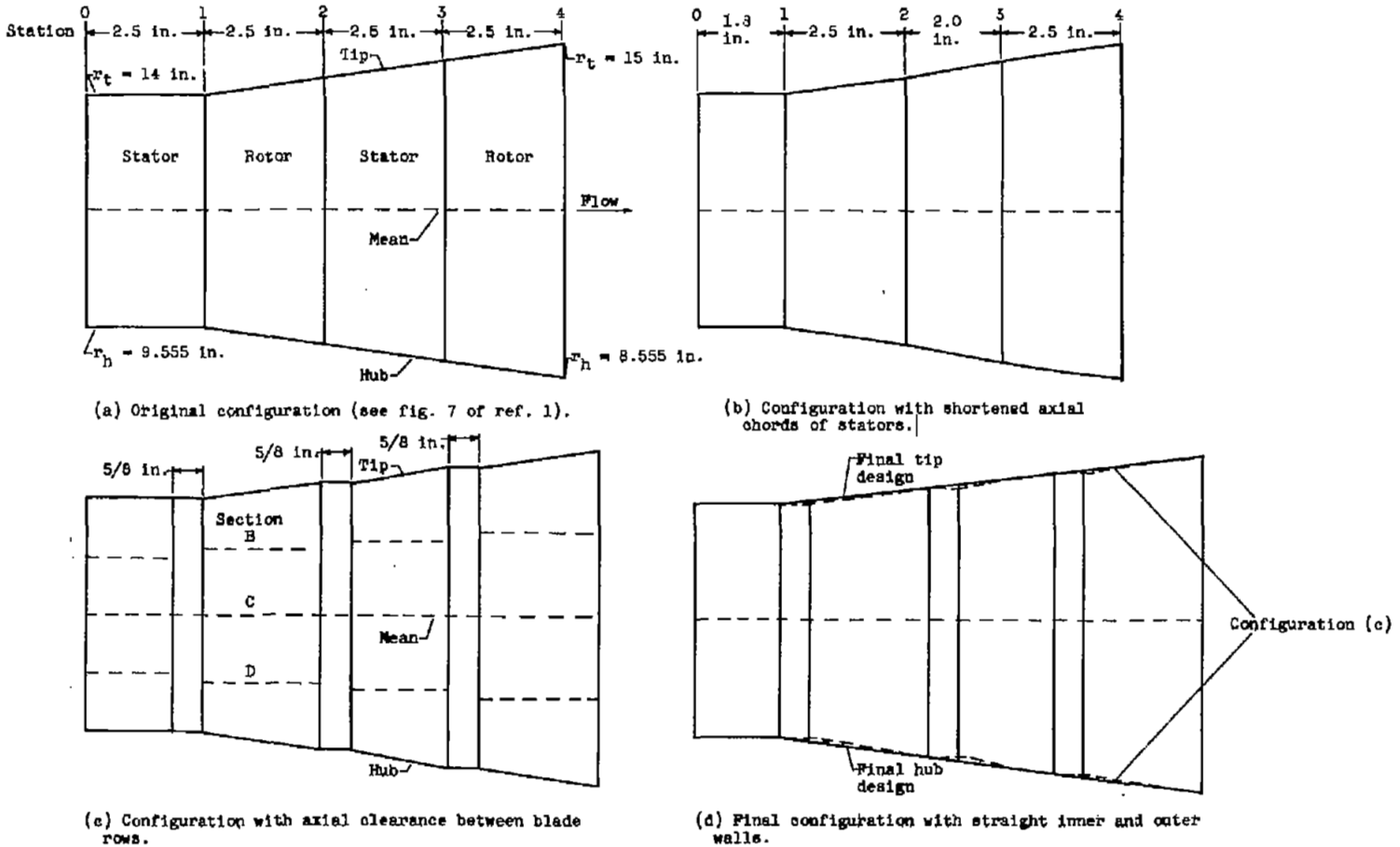

Figure 2. - Progressive design changes of inner and outer wall configuration.

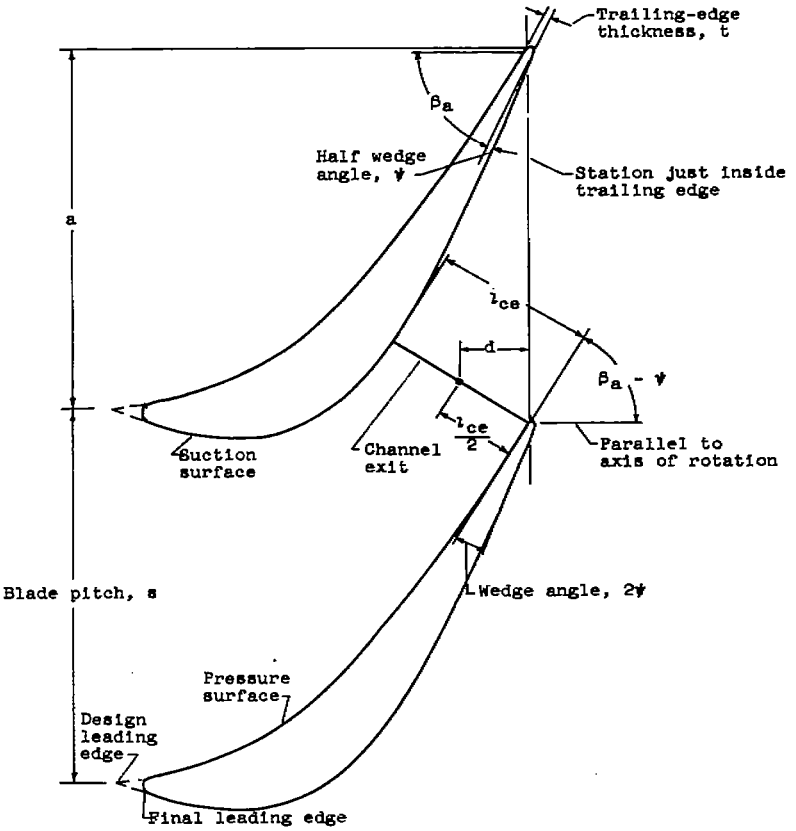

(a) Stator blades.

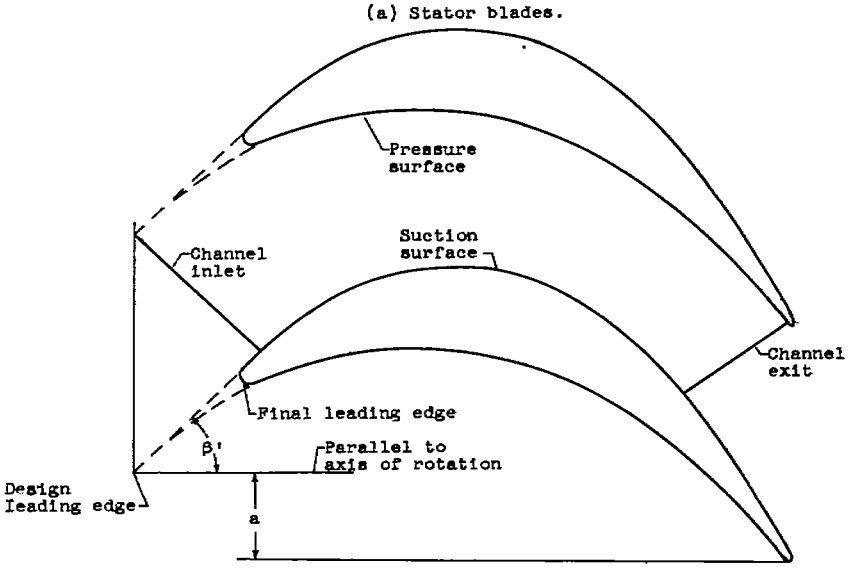

(b) Rotor blades. (Variables not shown are same as for stator blades.)

Figure 3. - Some blade design variables at leading and trailing edges.

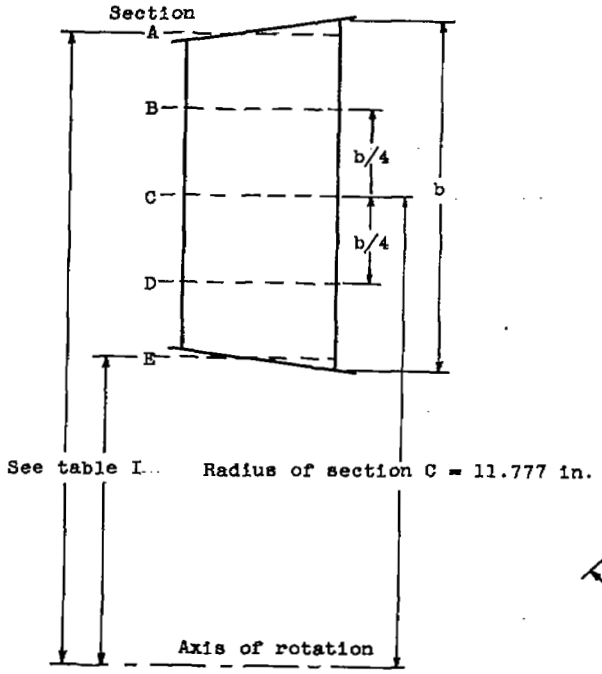

(a) Typical blade, side view (except for first-stage stator, which has constant hub and tip radii).

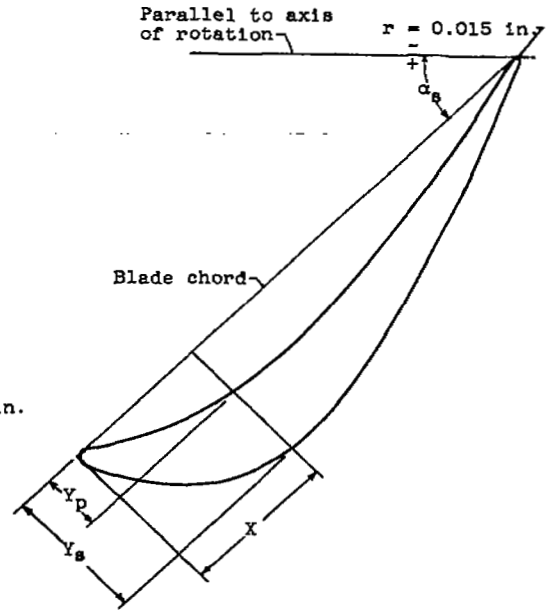

(b) Stator blade section, top view.

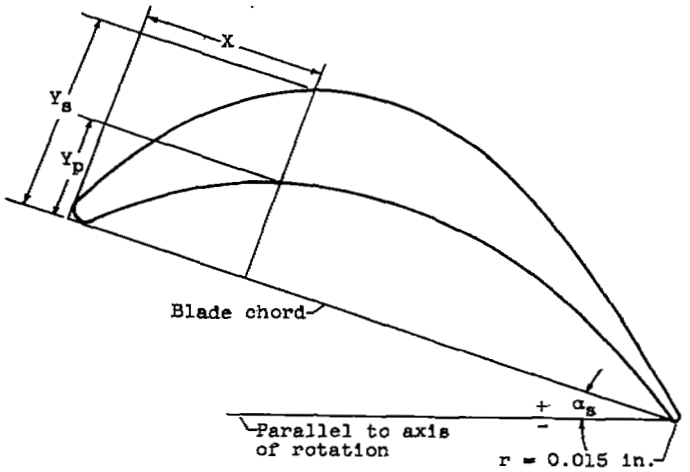

(c) Rotor blade section, top view.

Figure 4. - Typical top and side views of stator and rotor blades for use with table I.

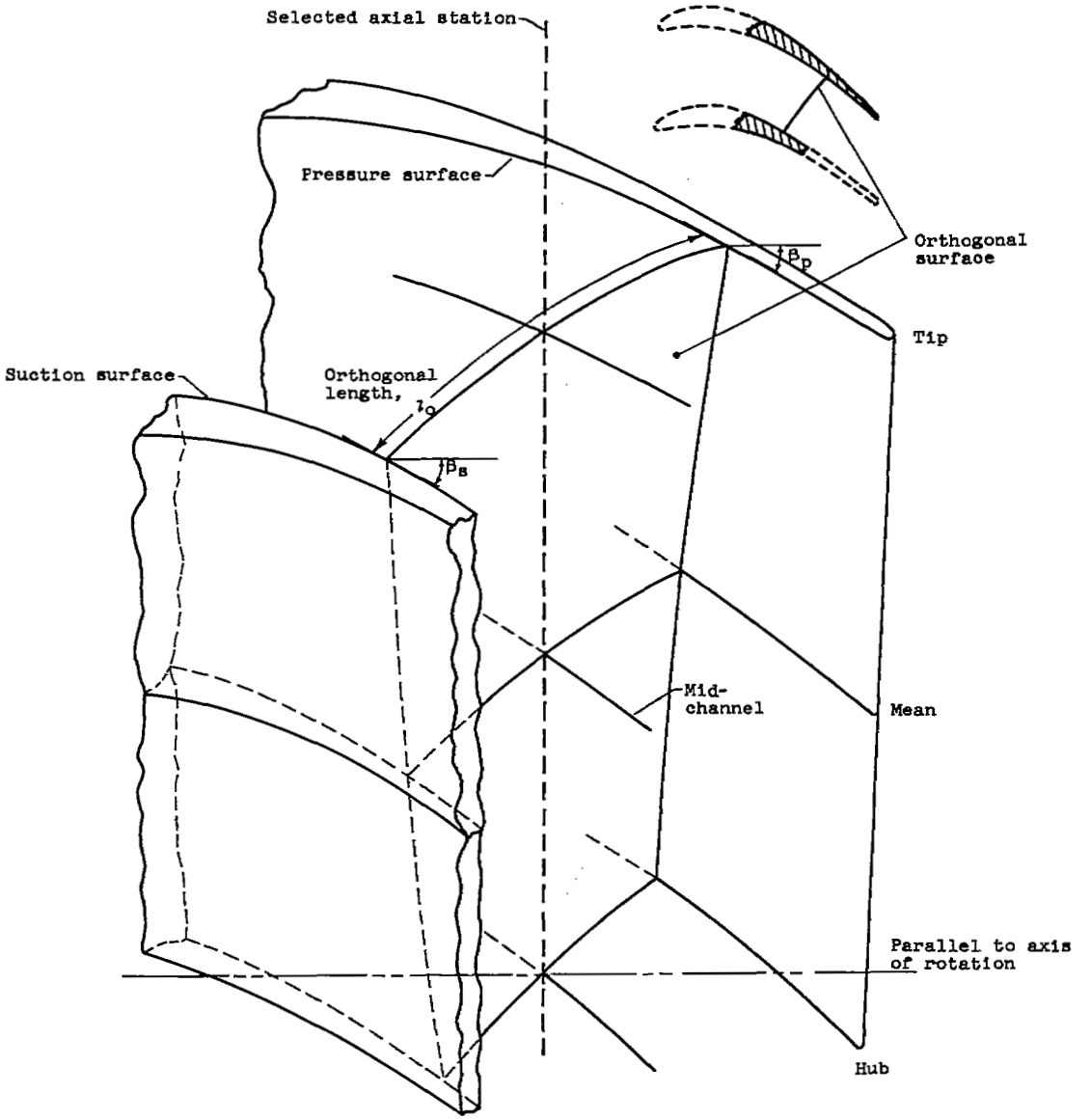

Figure 5. - Description of orthogonal surface and some variables in design procedure.

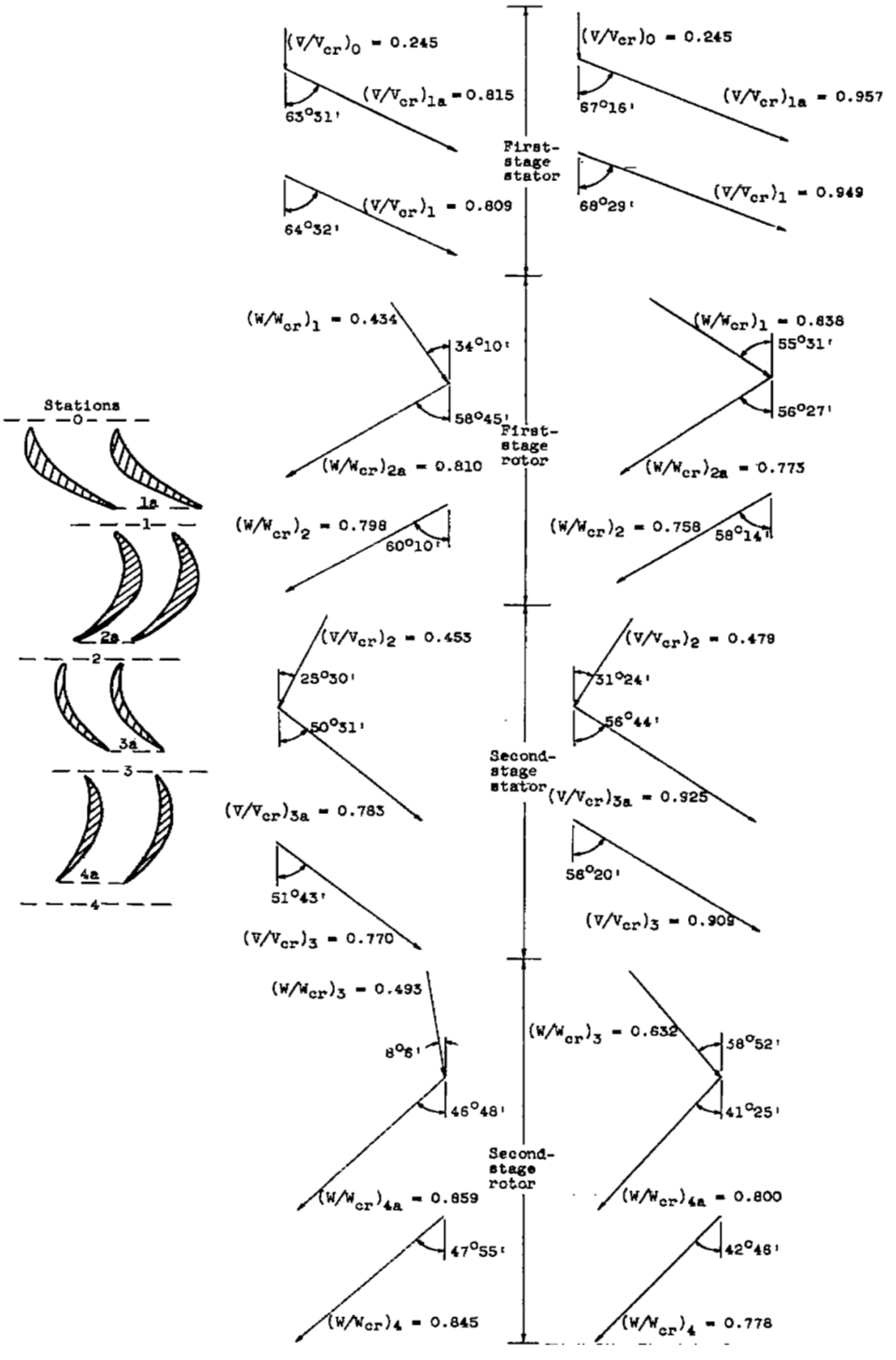

(a) Section B. (b) Section D.

Figure 6. - Velocity diagrams used in design of blades for two-stage turbine. (See fig. 4(a) for location of sections.)

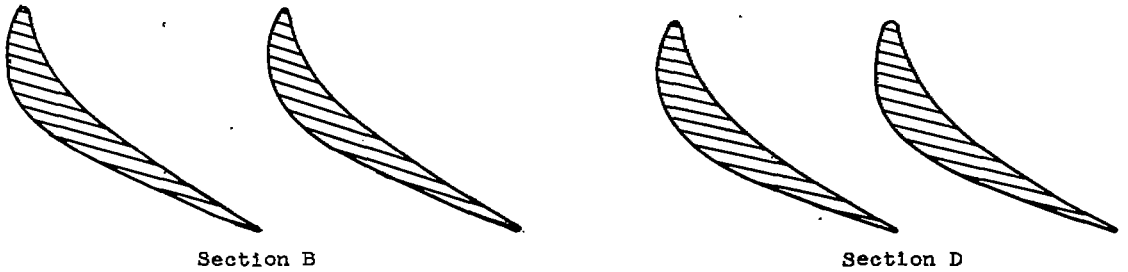

(a) First-stage stator.

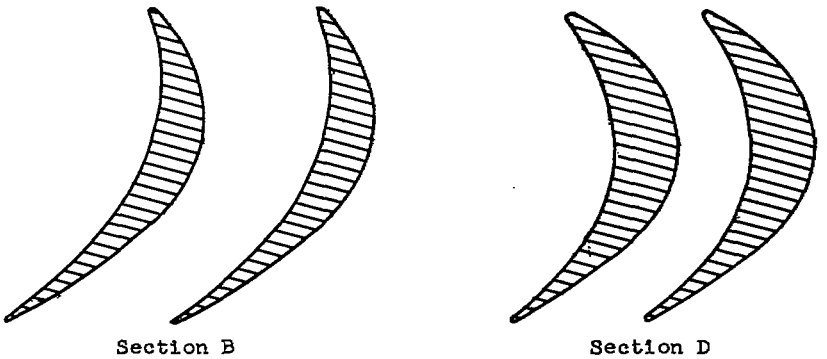

(b) First-stage rotor.

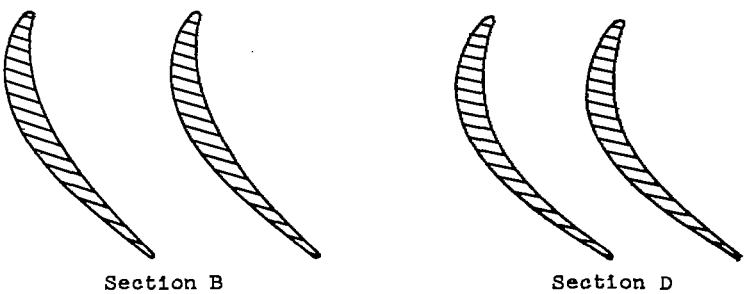

(c) Second-stage stator.

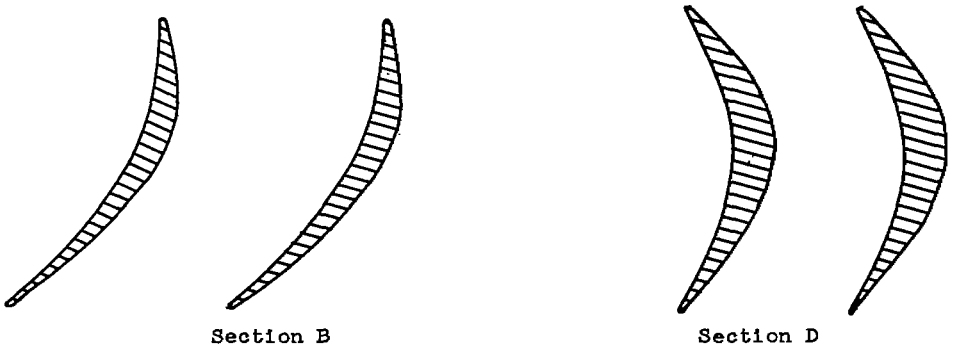

(d) Second-stage rotor.

Figure 7. - Blade profiles of stator and rotor blades.
(See fig. 4(a) for location of sections.)

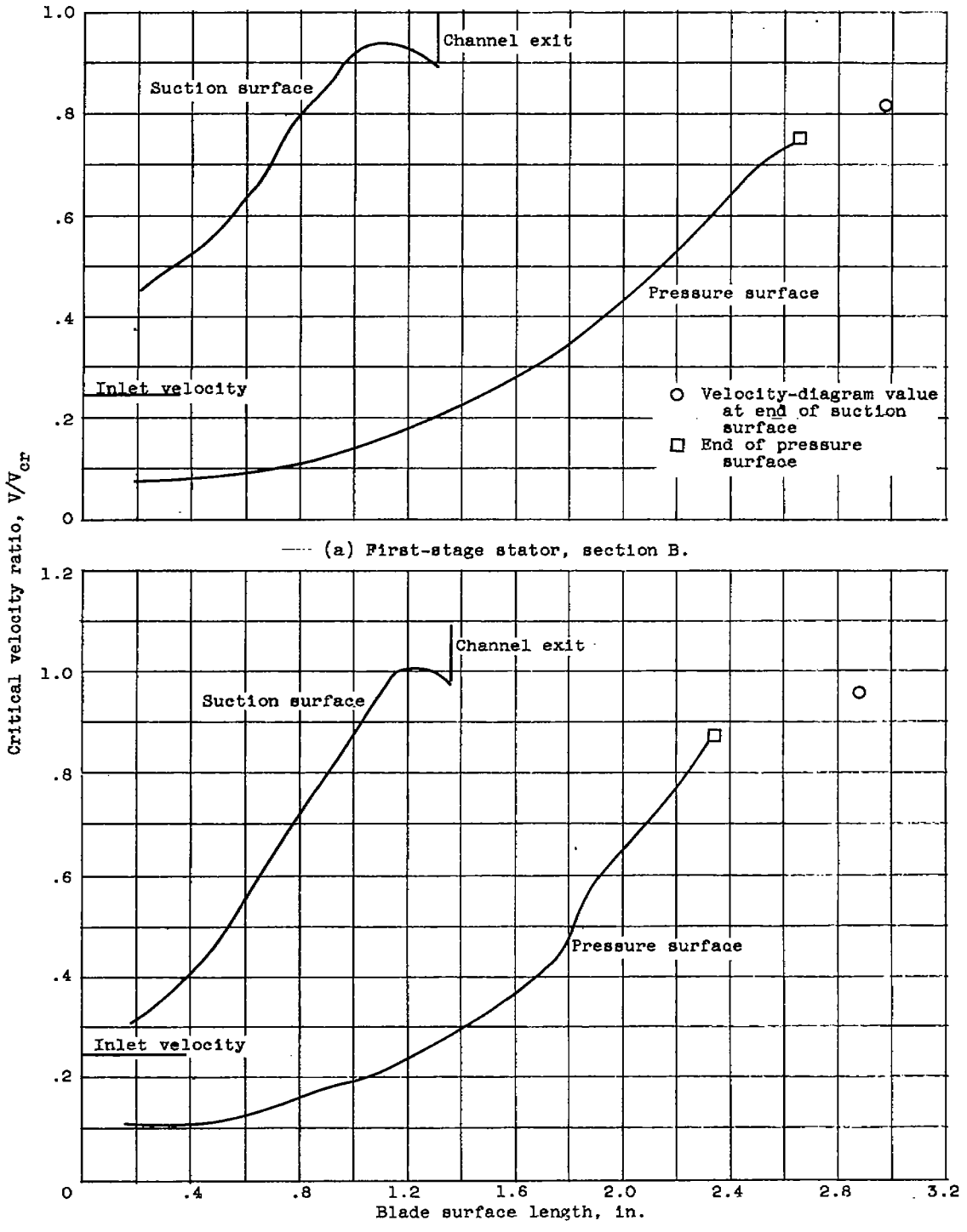

(a) First-stage stator, section B.

(b) First-stage stator, section D.

Figure 8. - Design surface velocity distributions at blade sections B and D for all four blade rows.

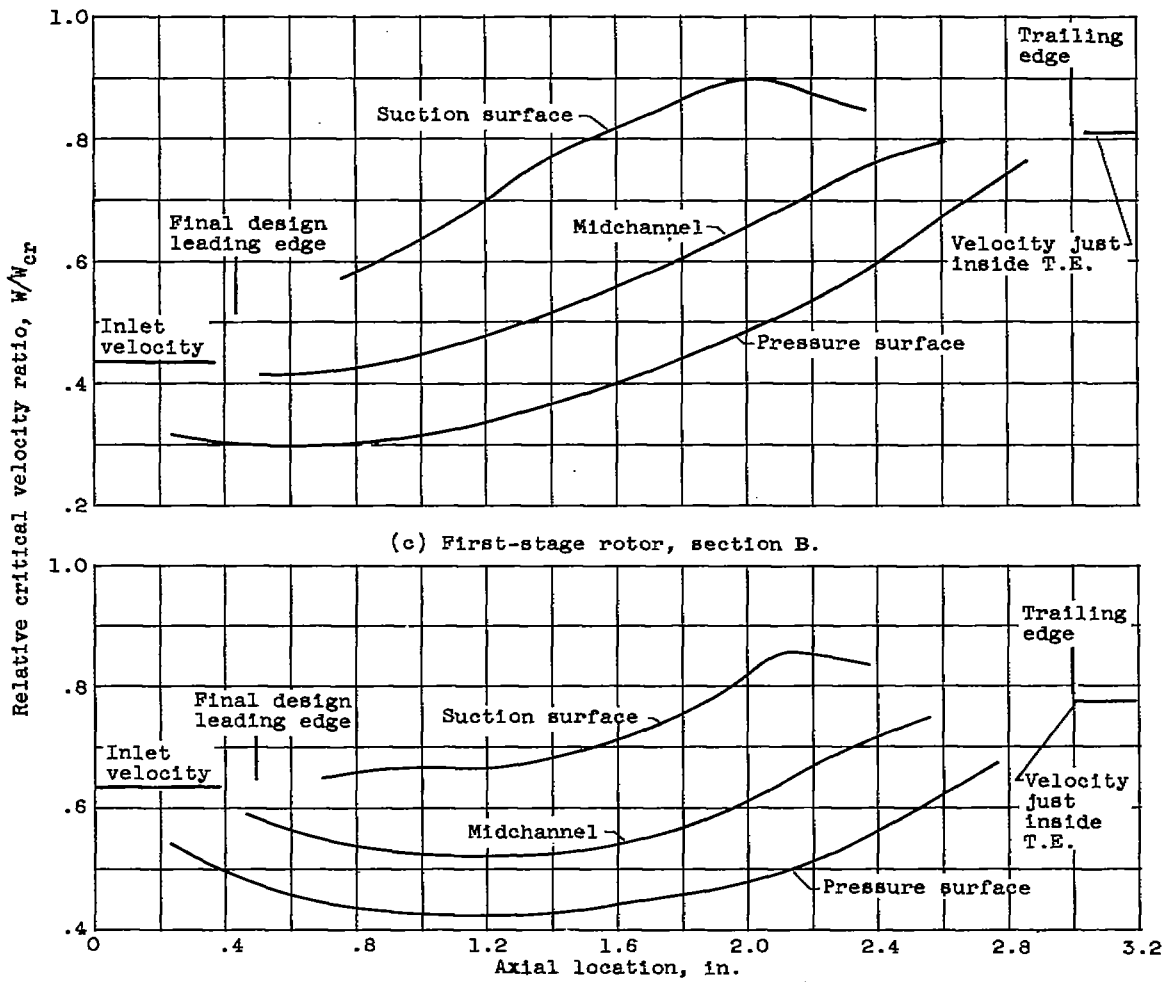

(c) First-stage rotor, section B.

(d) First-stage rotor, section D.

Figure 8. - Continued. Design surface velocity distributions at blade sections B and D for all four blade rows.

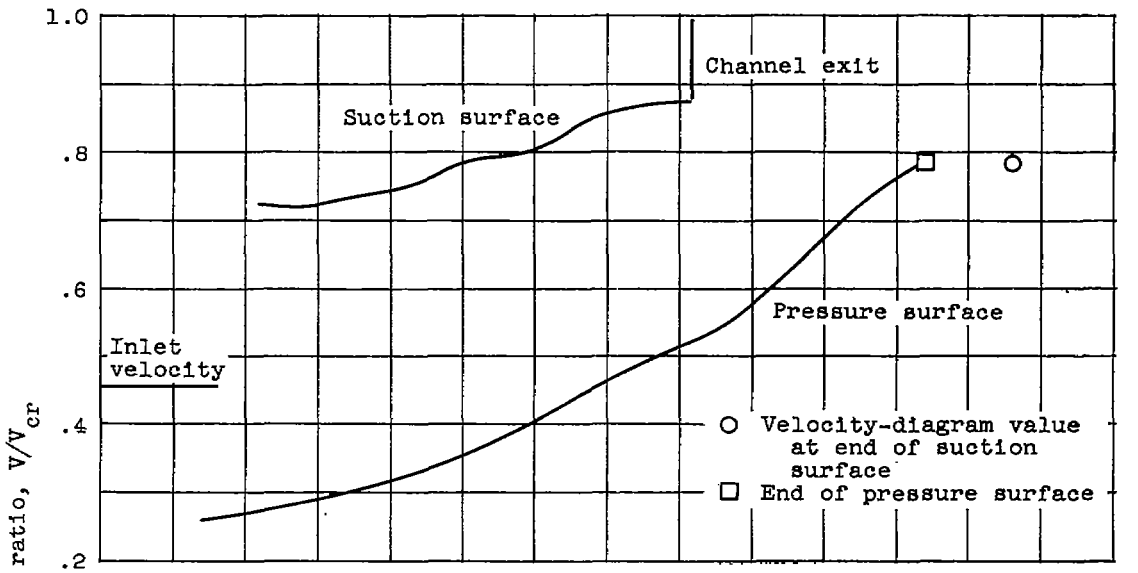

(e) Second-stage stator, section B.

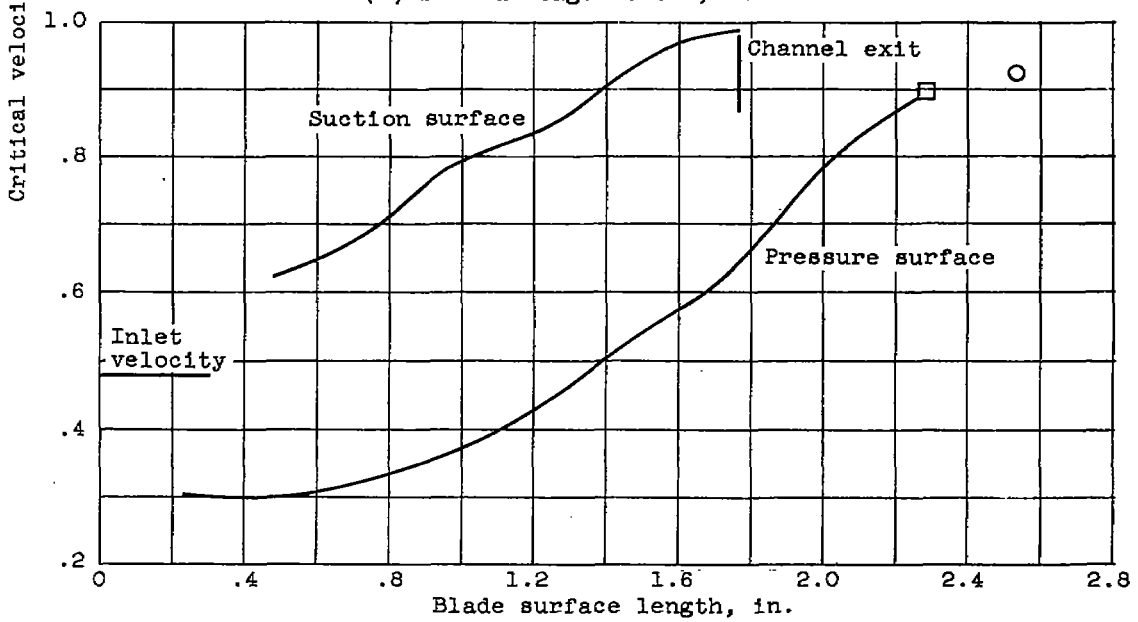

(f) Second-stage stator, section D.

Figure 8. - Continued. Design surface velocity distributions at blade sections B and D for all four blade rows.

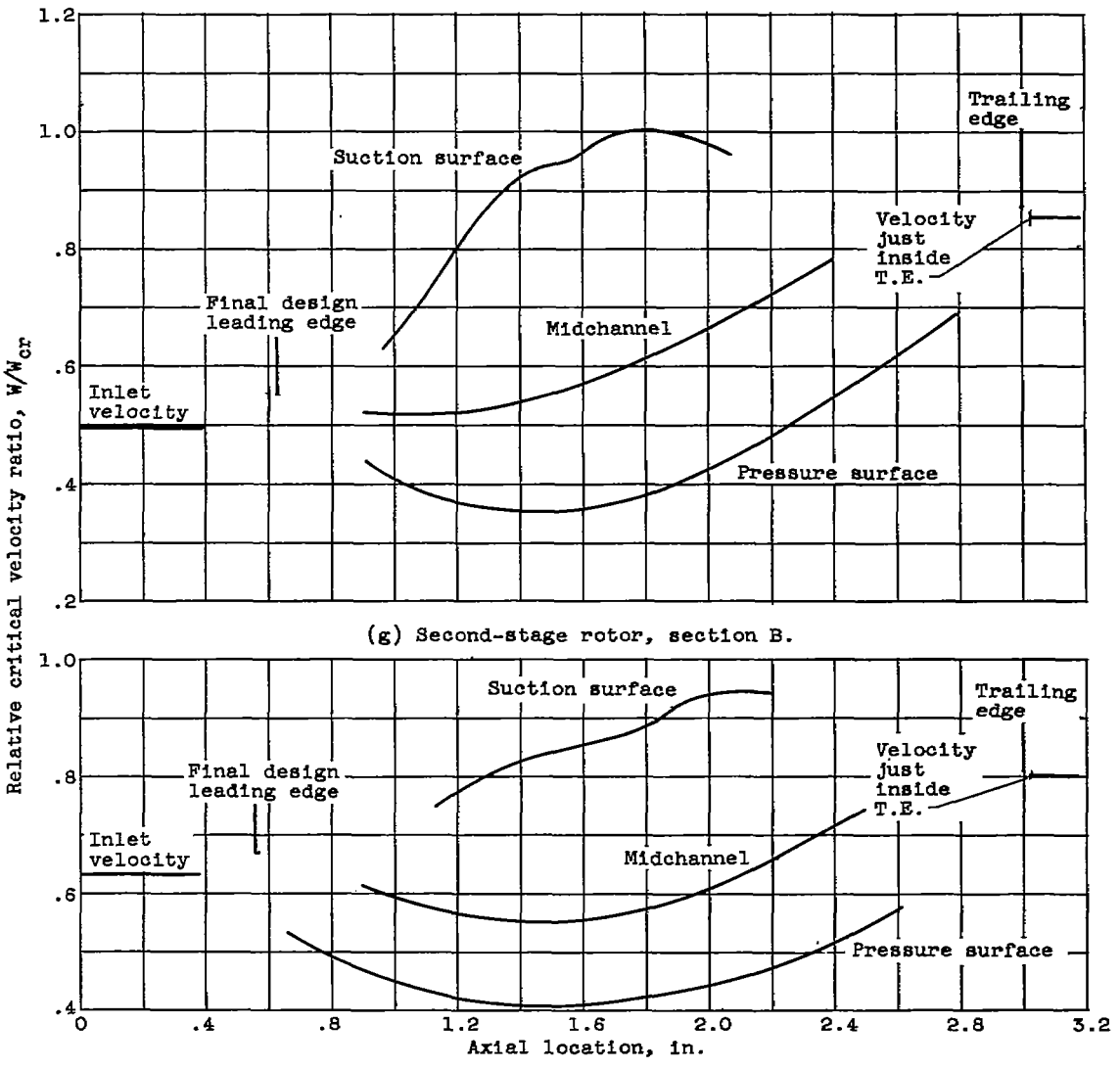

(g) Second-stage rotor, section B.

(h) Second-stage rotor, section D.

Figure 8. - Concluded. Design surface velocity distributions at blade sections B and D for all four blade rows.